ACS APPLIED MATERIALS & INTERFACES

Research Article

www.acsami.org

Biomineralization of Stable and Monodisperse Vaterite Microspheres Using Silk Nanoparticles

Lijie Liu,[†] Xiuli Zhang,[†] Xi Liu,[†] Jing Liu,*[,‡] Guozhong Lu,[§] David L. Kaplan,[†,∥] Hesun Zhu,[⊥] and Qiang Lu*[,†]

[†]National Engineering Laboratory for Modern Silk & Collaborative Innovation Center of Suzhou Nano Science and Technology, Soochow University, Suzhou 215123, People's Republic of China

[‡]Regenerative Medicine Center, First Affiliated Hospital of Dalian Medical University, No. 222 Zhong Shan Road, Dalian 116011, People's Republic of China

[§]Department of Burns and Plastic Surgery, The Third Affiliated Hospital of Nantong University, Wuxi 214041, People's Republic of China

[∥]Department of Biomedical Engineering, Tufts University, Medford, Massachusetts 02155, United States

[⊥]Research Center of Materials Science, Beijing Institute of Technology, Beijing, 100081, People's Republic of China

Supporting Information

ABSTRACT: The influence of silk fibroin (SF) on calcium carbonate ($CaCO_3$) biomineralization has been investigated; however, the formation of small, uniform SF-regulated vaterite microspheres has not been reported. In this work, spherical $CaCO_3$ was synthesized via coprecipitation in the presence of SF. SF nanostructures were first tuned by self-assembly at 60 °C to provide better control of the nucleation of $CaCO_3$. Subsequently, monodisperse vaterite microspheres about 1.1 μm were generated by controlling aggregation and growth of $CaCO_3$ under appropriate concentrations of SF and Ca ions. In contrast to unstable vaterite, the microspheres generated in the present study have sufficient stability in aqueous solution for at least 8 days without transformation into calcite, due to the electrostatic interactions between the Ca ions and the preassembled SF nanostructures. The microspheres as drug carriers of doxorubicin (DOX) were assessed and found to have good encapsulation efficiency, sustained drug release without burst release, and pH sensitivity. These new SF/$CaCO_3$ hybrids may provide new options for various biomedical applications.

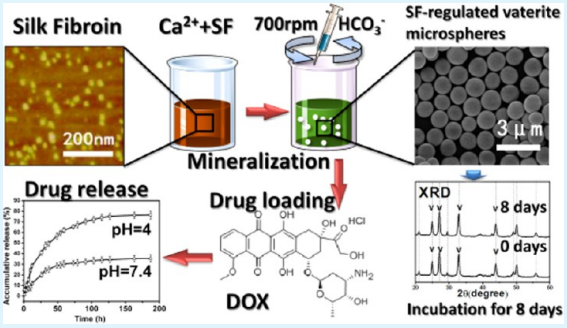

KEYWORDS: *silk, vaterite, biomaterials, pH sensitivity, drug release*

1. INTRODUCTION

Biominerals, such as oyster shells, corals, ivory, bone, and enamel, originate from complex hierarchical structures with combinations of organic and inorganic components to achieve extraordinary optical and mechanical properties for different biological functions.[1−6] Inspired by these extraordinary properties, biomimetic synthesis of organic−inorganic hybrid materials has been of ongoing interest due to the need for low-cost and environmentally friendly approaches to process advanced functional materials.[7−11] Remarkably, these mineral phases are generated at ambient environmental conditions of temperature, pressure, and water, without the need for high cost and intensive processing methods.

Calcium carbonate is a scientifically and industrially important mineral since it is present in different living organisms for protection or structural support[12−15] and also has been widely used in many industries for papermaking, plastics, paints, cosmetics, and recently pharmaceutical applications.[16−18] Previous studies have confirmed the important role of macromolecules in the fabrication of biominerals, including the relationship between the functional properties, organic−inorganic interfaces, and the hierarchical architectures.[19−21] These insights have resulted in approaches to artificially synthesize calcium carbonate with specific superstructures to achieve superior properties when compared to traditional engineered calcium carbonate formed at high temperatures and pressures.[22−24]

Although calcium carbonate materials with various morphologies have been biomimetically synthesized using polysaccharides, proteins, polyelectrolytes, and synthetic polymers as crystal growth modifiers,[25−28] few of these have a regular structure or match the mechanical properties of the native analogue. Recently, due to the similarity in amino acid composition between SF and silk-like proteins in the nacreous shell layer of mollusks and its better biocompatibility, SF has been used to synthesize calcium carbonate crystals.[29−36] These

Received: October 22, 2014
Accepted: January 12, 2015
Published: January 12, 2015

DOI: 10.1021/am507309t
ACS Appl. Mater. Interfaces 2015, 7, 1735−1745

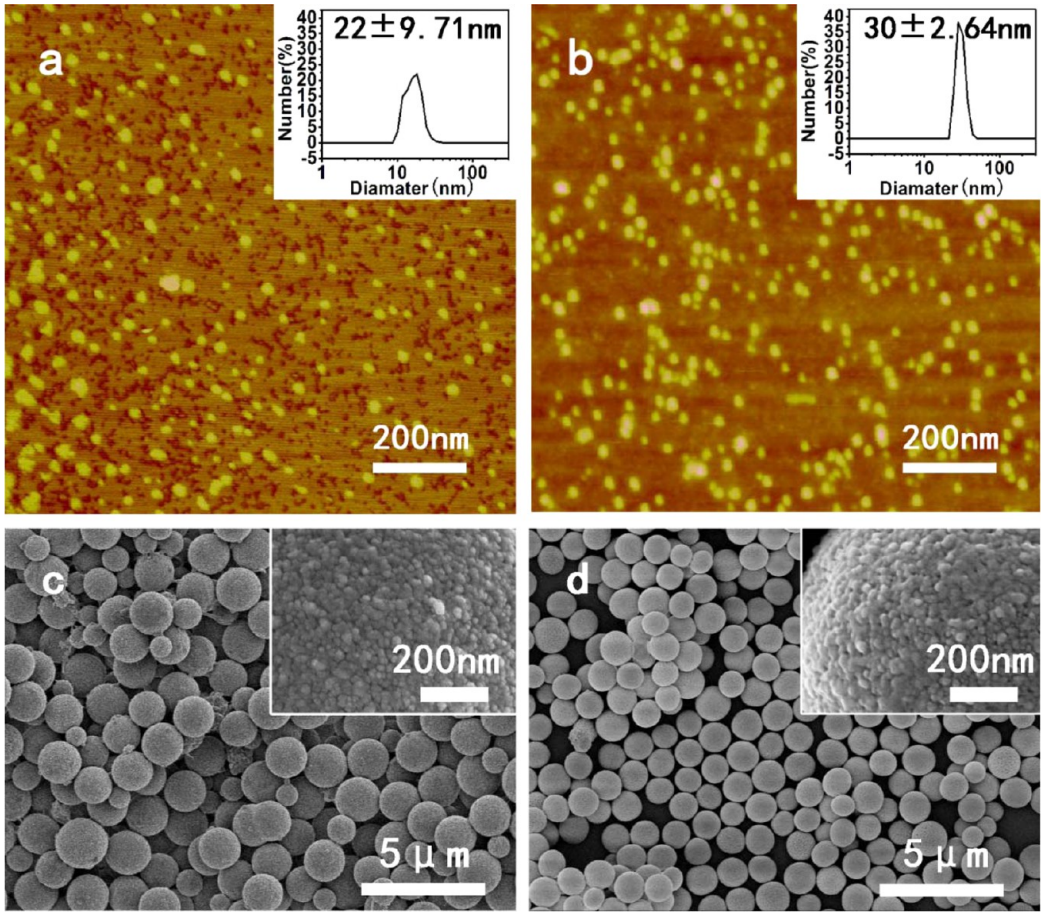

Figure 1. Morphologies of SF templates and SF-regulated $CaCO_3$ microspheres: (a) AFM image of SF in fresh solution, (b) AFM image of SF after treatment for 24 h at 60 °C, (c) SEM image of $CaCO_3$ with fresh SF (a) as template, and (d) SEM image of $CaCO_3$ with treated SF (b) as template. (Insets in a and b) Size distribution of the different SF nanoparticles. (Insets in c and d) Magnified image of the different $CaCO_3$ microspheres.

studies are attracting great interest due to the possibility of the SF−$CaCO_3$ system as a model in biomineralization and the promising application future of SF-regulated $CaCO_3$ particles in biomedical field. They indicated that SF effectively controlled the morphology, orientation, and crystal polymorph of $CaCO_3$;[34,36] however, challenges remain in the preparation of $CaCO_3$ particles with homogeneous structures and with pure polymorph. Recently, monodisperse vaterite particles with an ordered nanostructure was successfully fabricated with SF via the use of compressed CO_2, implying the possibility to control the morphology and polymorph of SF-regulated $CaCO_3$.[38,39] Unfortunately, the size of the vaterite particles in this process was above 10 μm, unsuitable for many industrial applications such as for drug carriers and tissue regeneration.[35,37] Although the critical function of SF in regulating $CaCO_3$ morphology and polymorph was confirmed,[35,37] there are no reports on further improvements of polymorphic control of $CaCO_3$ by fabricating nanostructures of the SF modifier. Therefore, a facile method to achieve such polymorph control of uniform $CaCO_3$ particles through the structure of SF was the goal in the present study.

Unlike previous studies, the nanostructures of SF were first regulated in our strategy to provide better template and modifier for the following biomineralization. SF with controllable nanostructures and secondary conformations have been generated via regulating the self-assembly process.[40] Herein, we report a simple, rapid approach for the synthesis of near monodisperse vaterite particles using homogeneous SF nanoparticles as modifiers. Compared with previous approaches to regulate the formation of $CaCO_3$ particles by different polymers,[41−43] the size of the particles in the present study was reduced to about 1 μm, which is more suitable for many applications. Further, unlike previous metastable analogues, the vaterite polymorph was stabilized in air and water environments due to the stabilizing function of the SF. Therefore, the present study provides an effective way to prepare $CaCO_3$ particles with control and also offers new insights into the functions of SF in biomimetic mineralization processes.

2. EXPERIMENTAL SECTION

2.1. Materials. Calcium chloride ($CaCl_2$) and ammonium bicarbonate (NH_4HCO_3) (Sinopharm Chemical Reagent Co. Ltd., Beijing, People's Republic of China) were of analytical grade and used without further purification. Deionized water used in all experiments was obtained from a Milli-Q system with resistivity greater than 18.2 MΩ cm. Doxorubicin hydrochloride (DOX) was purchased from Beijing HuaFeng United Technology Co., Ltd., China. All glass was cleaned and sonicated in ethanol for 10 min, further soaked with a H_2O−HNO_3(65%)−H_2O_2(1:1:1 by volume) solution, rinsed with deionized water and acetone, and then dried in air.

2.2. Preparation of SF Nanoparticles. SF solutions were prepared according to our previously established procedures.[44] *Bombyx mori* silk fibers were boiled for 20 min in an aqueous solution of 0.02 M Na_2CO_3 and then rinsed thoroughly with distilled water to extract the sericin proteins. Then the extracted SF was dissolved in 9.3 M LiBr solution at 60 °C for 4 h, yielding a 20 w/v% solution. The solution was dialyzed against distilled water using a dialysis tube

DOI: 10.1021/am507309t
ACS Appl. Mater. Interfaces 2015, 7, 1735−1745

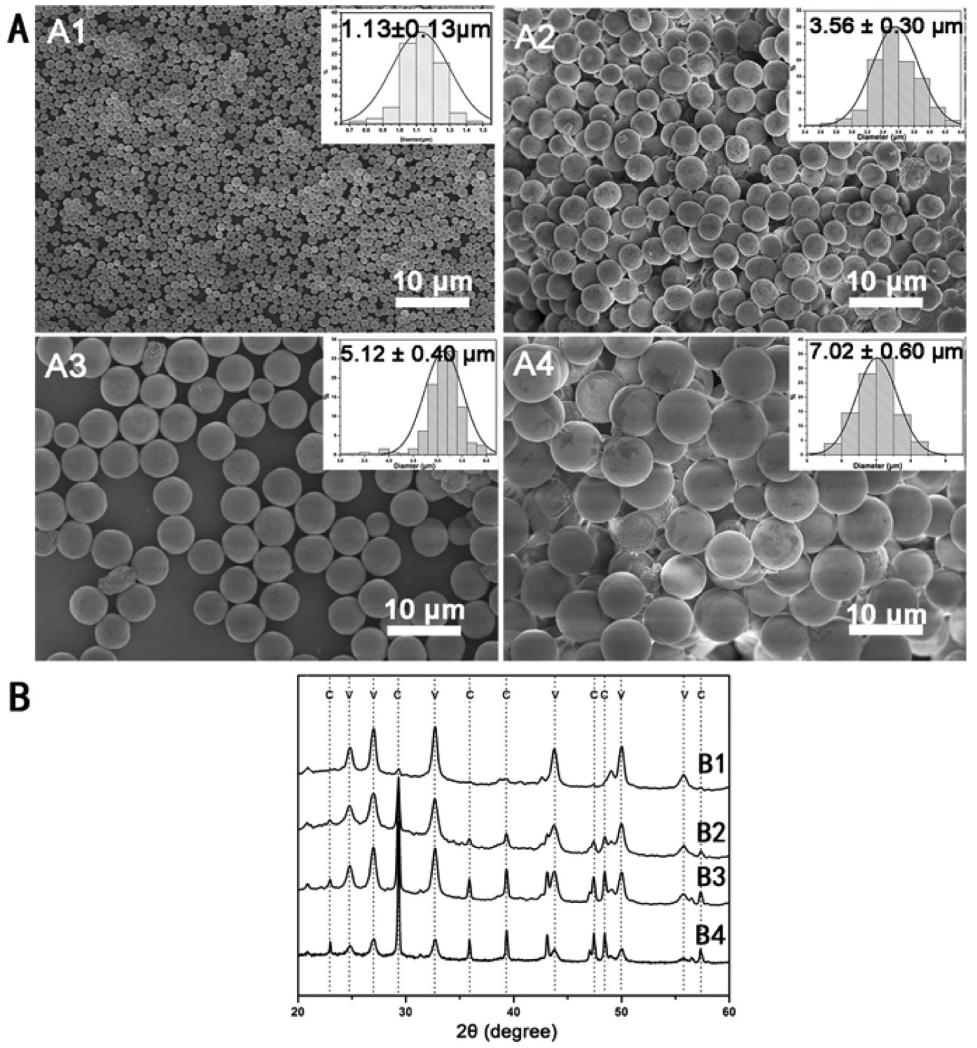

Figure 2. SEM images (A) and XRD patterns (B) of $CaCO_3$ particles obtained under constant SF concentration (4 wt %) and various Ca ion concentrations. Ca ion concentrations were as follows: (A1, B1) 0.27, (A2, B2) 0.36, (A3, B3) 0.54, and (A4, B4) 1.08 mol/L. (Insets in A) Size distribution of the $CaCO_3$ particles.

(Pierce, molecular weight cutoff 3500) for 3 days to remove the salt. The dialyzed solution was centrifuged at 9000 rpm for 20 min to remove silk aggregates formed during the process. The final concentration of aqueous SF solution was about 7 wt %, determined by weighing the remaining solid after drying. The fresh solution was sealed at 60 °C for 24 h to induce nanoparticle formation (Figure 1b) based on our recent study.[40]

2.3. Preparation of SF-Regulated Vaterite Microspheres. SF-regulated vaterite microspheres were prepared by direct mixing of NH_4HCO_3 solution with the solution containing $CaCl_2$ and SF nanoparticles. In a typical synthesis, $CaCl_2$ solution (0.27 mol/L, 5 mL) was added into aqueous SF (4 wt %, 15 mL) and kept quiescent for 30 min. Then an aqueous solution of NH_4HCO_3 (0.54 mol/L, 5 mL) was injected into the blend solution under vigorous stirring at 700 rpm based on our preliminary study. After stirring for about 10 min, the solution was allowed to stand for 1 h at room temperature. SF-regulated vaterite microspheres were obtained by centrifuging the experiential suspension and washing three times with deionized water. Samples were dried at room temperature for further characterization. SF and $CaCl_2$ solutions with different concentrations were also used to prepare $CaCO_3$ particles with various morphologies through the same process. The structure changes of the $CaCO_3$ following the increase of reaction time was investigated by controlling the different reaction time after the injection of the NH_4HCO_3 solution and then centrifuging the experiential suspension and washing three times with deionized water.

2.4. Loading and Release of DOX in the $CaCO_3$ Microspheres. Twenty milligrams of the $CaCO_3$ microspheres was added into 2 mL of DOX aqueous solution (0.5 mg/mL). The mixture was shaken in the thermostatic shaker for 24 h at 25 °C. Then the products were collected by centrifugation at 6000 rpm for 10 min, washed twice with 1 mL of deionized water, and dried at room temperature for future use. The DOX content of the supernatant was determined by measuring the absorbance at 486 nm with a microplate reader (Synergy H1, BioTek, VT, USA) based a calibration curve. The loading content and entrapment efficiency of DOX was calculated as follows

$$\text{Drug loading content} = (W_T - W_F)/W_{CM} \times 100\%$$

$$\text{Entrapment efficiency} = (W_T - W_F)/W_T \times 100\%$$

where W_T is the total weight of DOX in the reaction, W_F is the total weight of free DOX remaining in the supernatant, and W_{CM} is the total weight of the $CaCO_3$ microspheres loaded with DOX. The data are presented as mean ± standard deviation (SD) based on the triplicate measurements of the different samples.

For drug release studies, 20 mg of the dried DOX-loaded $CaCO_3$ microspheres after washing treatment was added into 2 mL of PBS solution at different pH values (4 and 7.4) and placed in a thermostatic

DOI: 10.1021/am507309t
ACS Appl. Mater. Interfaces 2015, 7, 1735−1745

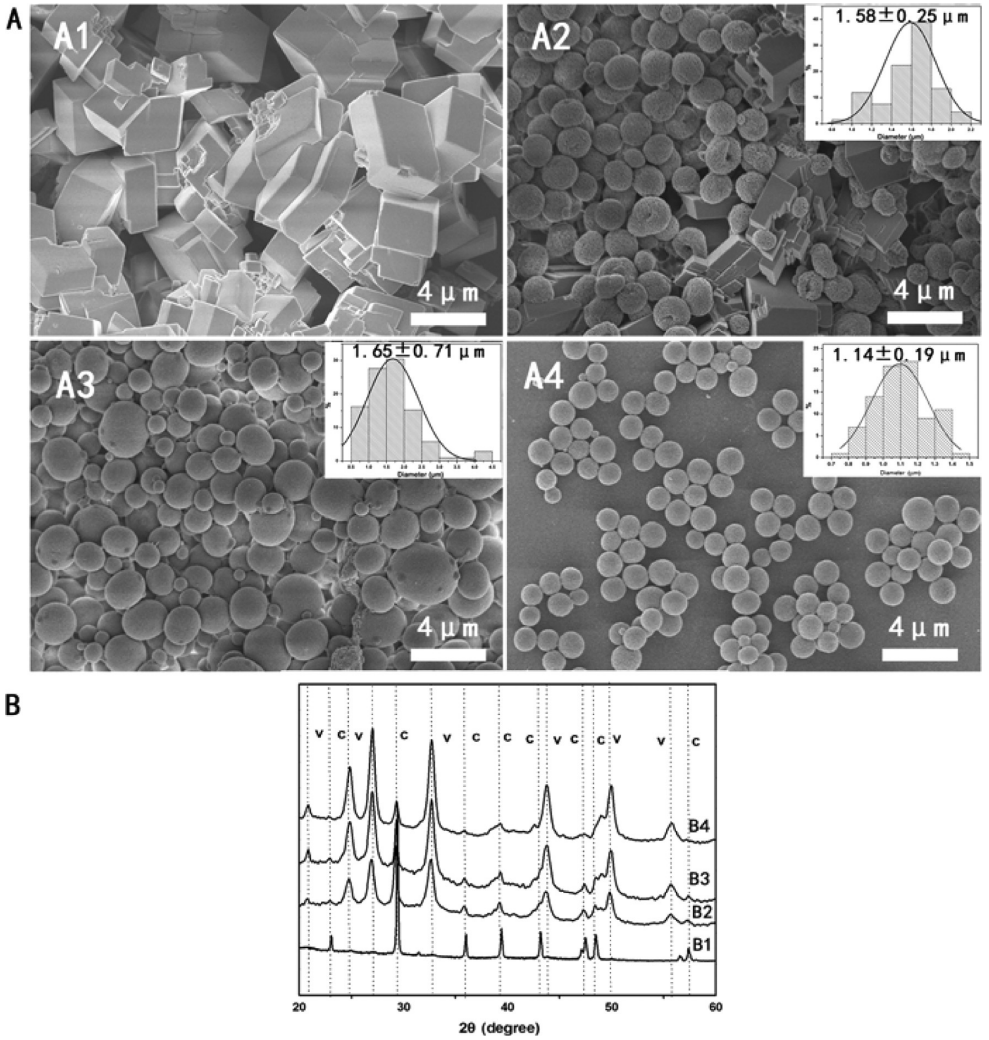

Figure 3. SEM images (A) and XRD patterns (B) of $CaCO_3$ particles obtained under constant Ca ion concentration (0.27 mol/L) and various SF concentrations. SF concentrations were as follows: (A1, B1) 0, (A2, B2) 0.1, (A3, B3) 1, and (A4, B4) 6 wt %. (Insets in A) Size distribution of the relative $CaCO_3$ particles.

shaker at 37 °C. At predetermined intervals, 1 mL of the supernatant was taken and analyzed by measuring the absorbance at 486 nm. The same volume (1 mL) of fresh PBS buffer at different pH values was added into the release medium. The release behaviors following the time were done based on one sample and repeated the release measurement in triplicate from different samples.

2.5. Characterization. The morphologies of $CaCO_3$ samples were characterized with scanning electron microscopy (SEM, S-4800, Hitachi, Tokyo, Japan). Energy-dispersive X-ray spectroscopy (EDAX, S-4800, Hitachi, Tokyo, Japan) was employed to determine elemental composition of the $CaCO_3$ microspheres. The samples were sputter coated with platinum and then measured with SEM at 5 kV. The nanostructure of SF template was studied with atomic force microscopy (AFM, Nanoscope V, Veeco, NY, USA). A 2 μL amount of the samples was dropped onto freshly cleaved 4 × 4 mm^2 mica surfaces and spin coated using a spin processor (WS-400, Laurell Technologies, PA, USA). A 225 μm long silicon cantilever with a spring constant of 3 N m^{-1} was used in tapping mode at 0.5 Hz scan rate. The images, element mapping, and selective area electron diffraction (SAED) patterns of the samples were further characterized with transmission electron microscopy (TEM, Tecani G2 F20 STwin, FEI, OR, USA) at 200 kV. The samples were embedded in epoxy resin (Fluka epoxy embedding kit, Sigma-Aldrich, St. Louis, MO, USA) according to standard procedures and sectioned into 300 nm slices with an Ultramicrotome (UC7-FC7, Leica, Solms, Germany). The sections were loaded on carbon-coated 300 mesh copper grids for measurement.

Fourier transform infrared spectroscopy (FTIR) was carried out with a Nicolet FTIR 5700 spectrometer (Thermo Scientific, FL, USA) in the range 4000−400 cm^{-1} to determine the presence of SF in the $CaCO_3$. The content of SF in the vaterite microspheres was measured through thermogravimetric analysis (TGA) (Diamond TG/DTA, PerkinElmer, MA, USA) at 10 °C min^{-1} in nitrogen gas with a flow rate of 40 cm^3 min^{-1}.

The polymorph of the $CaCO_3$ samples was assessed with X-ray diffraction (XRD). The XRD experiments were conducted with an X-ray diffractometer (X'Pert-Pro MPD, PANalytical, Almelo, Holland) with Cu Kα radiation at 40 kV and 30 mA and a scanning rate of 0.6°/min.

Fluorescence images of the DOX-loaded $CaCO_3$ microspheres were captured by a fluorescence inverted microscope (Axio Vert A1, ZEISS, Oberkochen, Germany).

3. RESULTS AND DISCUSSION

3.1. Effect of SF Microstructure on the Morphology of $CaCO_3$ Particles. SF nanospheres have been assembled under an electric field and then used to control spherical $CaCO_3$ particle growth.[28] Although only polydisperse $CaCO_3$ particles formed due to the dispersion of the SF nanospheres (100−500

DOI: 10.1021/am507309t
ACS Appl. Mater. Interfaces 2015, 7, 1735−1745

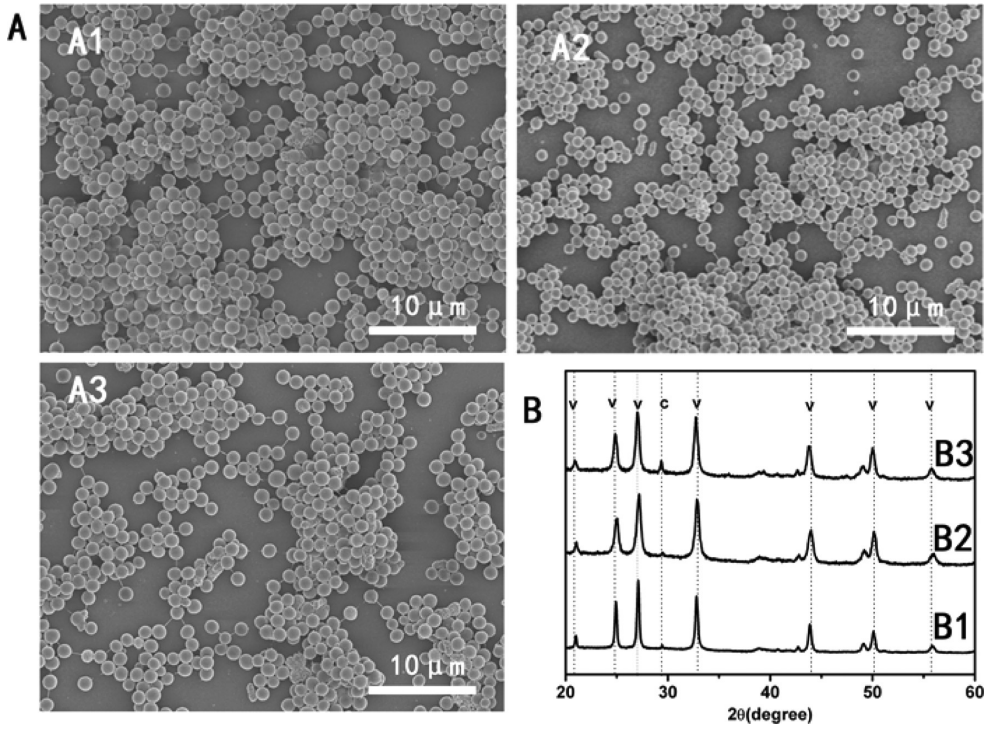

Figure 4. SEM images (A) and XRD patterns (B) of $CaCO_3$ particles at different reaction time points when the SF concentration and Ca ion concentration were 4 wt % and 0.27 mol/L, respectively: (A1, B1) 10 min, (A2, B2) 4 h, and (A3, B3) 8 h.

nm), the study implied the possibility of fabricating monodisperse spherical $CaCO_3$ particles if further control of the microstructure of the SF is achieved. Interestingly, SF nanospheres with improved homogeneous size could be self-assembled by culturing fresh SF for 24 h at 60 °C.[40] The nanospheres can be dispersed in aqueous solution for above 2 weeks without further aggregation. Compared to fresh solution (Figure 1a), the average size of the treated SF nanospheres was about 30 nm with a narrower size distribution (Figure 1b). The zeta potential of the nanospheres was −21.2 mV, which could provide sufficient charge interaction for the mineralization. Therefore, the $CaCO_3$ particles were prepared via a solution reaction process with the SF nanospheres as modifiers, achieving a more homogeneous morphology of $CaCO_3$ particles (Figure 1 d) with negative charge (zeta potential −7.6 mV).

Considering the influence of the component concentrations (SF and calcium) on the morphology of the $CaCO_3$ particles formed, the morphology of the $CaCO_3$ microspheres was further controlled by changing the Ca^{2+} and SF concentrations with the treated SF nanospheres as modifier. A direct dependence of crystal size and morphology on the concentration of Ca^{2+} at a constant initial SF concentration of 4 wt % was observed in representative images of $CaCO_3$/SF hybrids (Figure 2A). An increase of Ca^{2+} concentration in the range of 0.27−1.08 mol/L resulted in spherical $CaCO_3$ particles with increased diameters from 1 to 7 μm. Near monodisperse spherical particles were achieved with a Ca^{2+} concentration of 0.27 mol/L, while polydisperse particles were formed under the other reaction conditions. XRD patterns (Figure 2B) showed that the monodisperse spherical particles were vaterite, while the larger particles formed with higher Ca^{2+} concentrations were composed of vaterite and calcite.

Changing SF concentration at constant Ca^{2+} content (0.27 mol/L) also yielded different morphology changes. Typical rhombohedral calcite formed without SF as modifier, and then a mixture of rhombohedral calcite (Figure 3A1 and 3B1) and spherical and discal calcite/vaterite hybrids appeared with SF concentrations of 0.1 wt % (Figure 3A2 and 3B2). Following further increases of SF content (>1 wt %), all $CaCO_3$ particles transformed into spherical structures. Vaterite crystals also increased and became the only structure in the $CaCO_3$ spherical particles, accompanied by the increase of SF concentration from 1 to 6 wt %. Although vaterite was also the main crystal phase when SF concentration was 6 wt % (Figure 3A4 and 3B4), spherical vaterite particles with the lowest dispersion were achieved when the SF concentration was 4 wt % (Figure 2A1 and 2B1). Regulating the ratio of Ca^{2+} and SF as well as their concentrations was used to control the morphology and polymorph of $CaCO_3$.[32,34] In the present study, improved low dispersion of the $CaCO_3$ particles was also achieved via control of the two components to achieve almost pure vaterite microspheres with more homogeneous and smaller sizes than previously reported silk-regulated $CaCO_3$ particles.[36,38]

Time-resolved experiments were once performed under different CO_2 vapor diffusion methods to clarify the growth and crystallization process of $CaCO_3$. It was found that the reaction time was usually above 1 h for stable vaterite or aragonite formation in these processes.[34,35,37] In our study, the spherical vaterite particles formed within 10 min, significantly quicker than previously reported vapor diffusion methods.[34] The morphology and size of the spherical vaterite remained unchanged after 10 min (Figure 4A and 4B), indicating termination of the reaction. Therefore, through optimizing the nanostructure of the SF modifier and then tuning the concentrations of Ca^{2+} and SF, vaterite particles with improved

DOI: 10.1021/am507309t
ACS Appl. Mater. Interfaces 2015, 7, 1735−1745

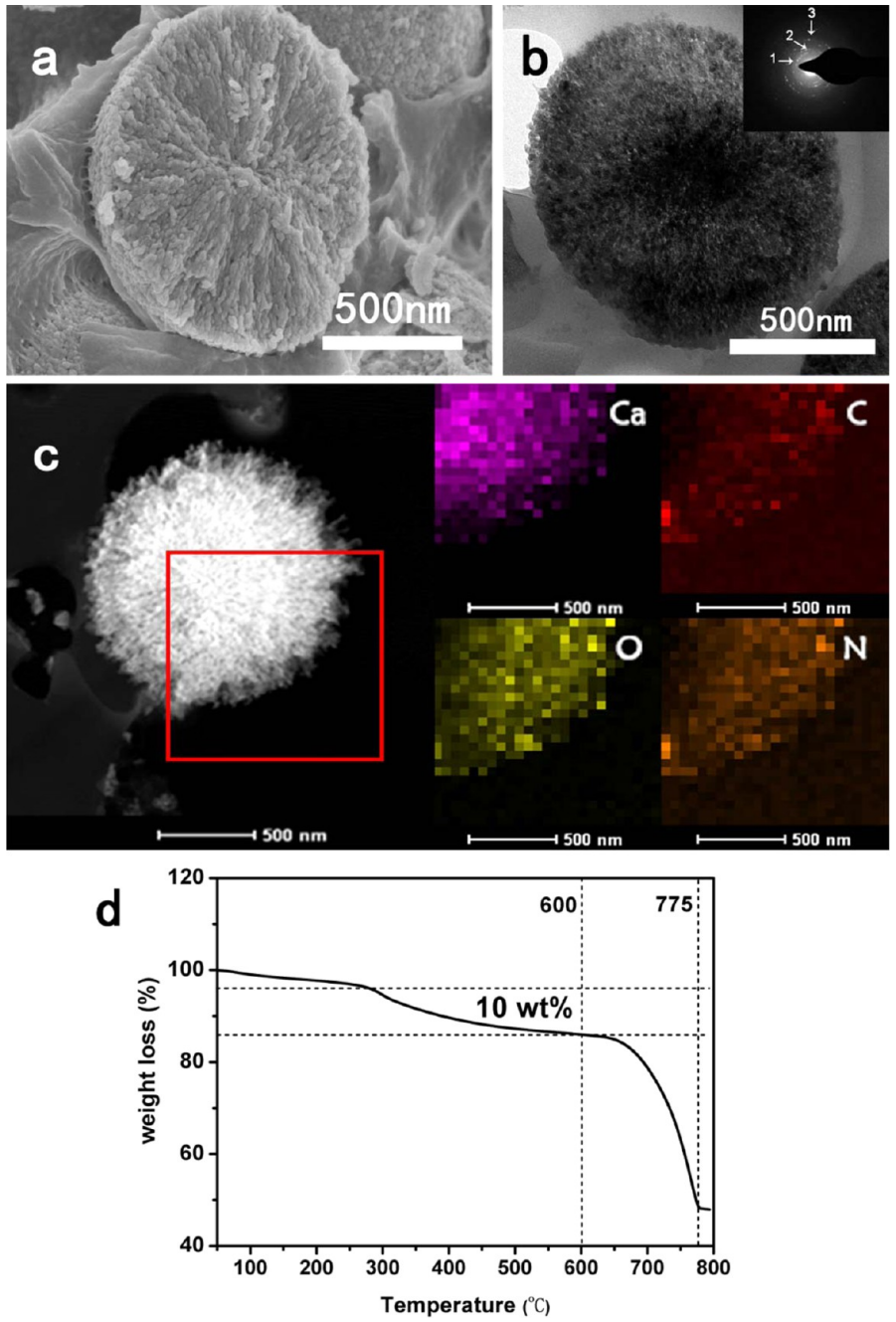

Figure 5. Microsphere nanocomposite structure and the SF distribution in the microspheres obtained in the presence of suitable SF and Ca ions (SF 4 wt %, Ca ion 0.27 mol/L): (a) SEM image of the sliced $CaCO_3$ at high magnification, (b) TEM image and SAED pattern of the $CaCO_3$ ultrathin section, (c) STEM and element mapping of the ultrathin section, and (d) TGA curve.

morphology and size were produced. The process also significantly reduce fabrication time compared with previously reported methods,[37] offering an effective approach to prepare significant quantities of specialized $CaCO_3$ particles.

3.2. Spherical Vaterite Formation Process. The $CaCO_3$ crystallization process in the presence of SF has been investigated in different studies.[29−37] Mechanistically, SF regulates amorphous $CaCO_3$ particle formation as a heterogeneous nucleator, followed by growth and aggregation of the crystal due to the strong interactions between Ca^{2+} and the charged amino acid residues in the SF chains.[33,35] The transformation of SF from random coil to β-sheet is considered a critical factor in the selection of $CaCO_3$ polymorph and ultimate morphology.[34,36] Recently, Xu prepared spherical vaterite particles via compressed CO_2 and proposed a possible mechanism.[38] They suggested that amorphous calcium carbonate aggregated and crystallized simultaneously with the assembly of parts of the SF chains to form disc-like particles and then grew into spherical vaterite, regulated by the remaining SF chains in solution. SF spontaneously transformed from random coil to beta-sheet without effective control in these processes, making it difficult to fabricate stable $CaCO_3$ particles with a specific morphology and polymorph.

Related to the present work, the nanostructure of SF in solution was regulated to form homogeneous nanoparticles,[44,45] providing more homogeneous template and then better control

DOI: 10.1021/am507309t
ACS Appl. Mater. Interfaces 2015, 7, 1735−1745

Scheme 1. Proposed Formation Process of the Vaterite Microspheres

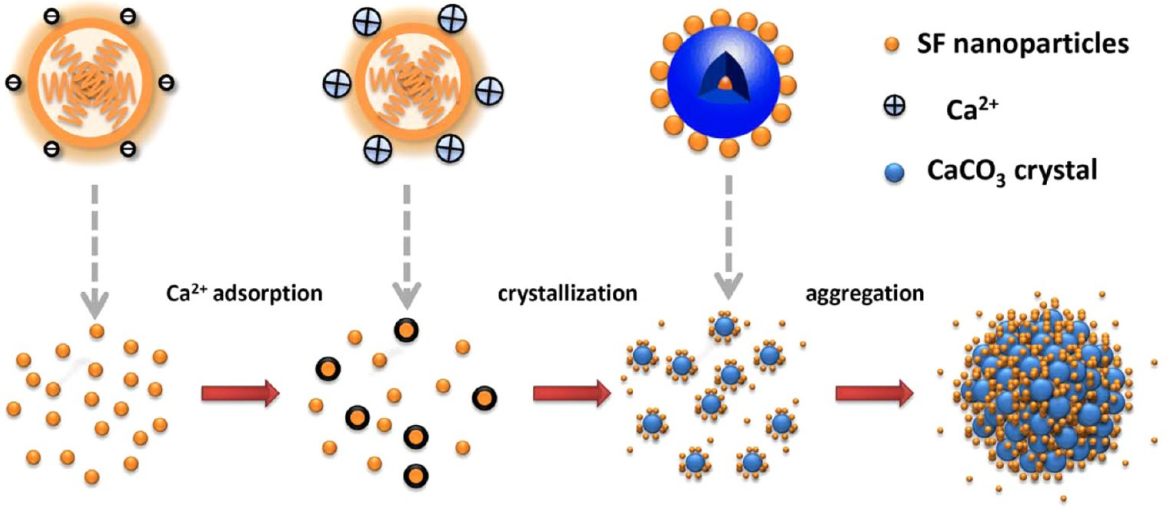

of the nucleator/modifier for $CaCO_3$ biomineralization. Similar to what happened in previous $CaCO_3$ crystallization processes in the presence of SF,[33] vaterite nanoparticles formed first with SF as the nucleator and then quickly aggregated to form larger particles to generate lower surface energy in a nonclassical passway.[46,47] Figure 5a shows that the $CaCO_3$ microspheres formed by the aggregation of many nanoparticles with 30−50 nm diameters. TEM images and SAED patterns further confirmed the existence of the nanoparticles as well as vaterite formation (Figure 5b). Different theories have been developed to explain the relationship between SF and the final morphology of the $CaCO_3$ particles,[33,36,38] with the assembly and transformation into beta-sheet critical for regulating oriented $CaCO_3$ aggregation.[34,36] Since homogeneous silk nanoparticles formed before $CaCO_3$ crystallization, non-oriented aggregation is preferred for the final assembly to spherical particles in the present study. Compared to previous results,[36] in the present work $CaCO_3$ microspheres stably aggregated even in low SF concentrations. Besides acting as a nucleator, SF also plays a key role in determining the final morphology and size of the particles. There is a strong dependence of the dispersity of microsphere sizes on the concentration of Ca^{2+} and SF, particularly at the mass ratio $[Ca^{2+}]$:[SF] = 1:4. The size of the $CaCO_3$ microspheres decreased with increasing SF concentration (Figure S1, Supporting Information), indicating that remanent SF in solution restricted crystallization growth as a polymer network. The near monodispersity of the $CaCO_3$ microspheres improved with an increase of SF concentration and achieved the lowest dispersity with a SF concentration of 4 wt %, declining with further increases in SF concentration (Figure S1, Supporting Information). It is not yet clear how to allocate SF as a nucleator and inhibitor in $CaCO_3$ biomineralization processes, SF morphology, secondary conformation, as well as content in the reaction system actively regulated the formation and dispersity of vaterite microspheres.

Without organic additives in mineralization processes, vaterite is kinetically preferred and forms first in supersaturated aqueous solution and then transforms to calcite via solvent-mediated dissolution−recrystallization processes.[48] Although some results have confirmed the stabilization effect of SF on the vaterite structure,[36] there is no effective way to prepare pure vaterite particles with SF as a modifier in a supersaturated aqueous solution. In the present study, the $CaCO_3$ microspheres composed of almost pure vaterite were achieved when the diameter was below 1.2 μm, while both vaterite and calcite appeared in microspheres with diameters above 1.5 μm (Figures 2 and 3). EDAX results revealed the nitrogen distribution both in the core (S_0) and the edge (S_1) areas of the vaterite microspheres, suggesting that SF was incorporated in the microspheres (Figure S2, Supporting Information). TGA and elemental mapping revealed the content and distribution of SF in the microspheres (Figure 5c and 5d). There was weight loss by TGA from 210 to 600 °C with a total weight loss of about 10%, ascribed to the thermal pyrolysis of the SF skeleton. The element mapping results showed a homogeneous distribution of SF inside the microspheres. These findings suggest that the silk must be closely packed with vaterite, providing sufficient stabilization to restrain the transformation from vaterite to calcite.

As shown in Scheme 1, some of the SF nanospheres induced vaterite nanoparticle formation at first, and then the remainder of the SF nanospheres further regulated the aggregation and growth to form the vaterite microspheres with a homogeneous size distribution. There seemed to be an upper size limitation to prepare vaterite microspheres in the present study, while in contrast only larger SF-regulated vaterite particles were achieved via the compressed CO_2 process.[38,39] A complicated SF-regulated crystallization process is suggested in our recent study, in which the growth and aggregation of $CaCO_3$ at different levels could occur simultaneously, resulting in the change of morphologies and crystal phases depending on reaction conditions.[33] The different growth and aggregation processes in the two methods might result in various distributions of SF inside the particles, endowing these vaterite microspheres with enough stability. Compared to the larger analogue, the homogeneous vaterite microspheres in the present study might offer utility in areas such as drug carriers, where such controlled size should allow better predictability in terms of release kinetics, targeting, and related needs.

3.3. Stability of SF-Regulated Vaterite Microspheres. Vaterite formation and stabilization remain key features due to its unique properties.[27,49] Therefore, the SF-regulated vaterite microspheres were incubated in a flowing water solution to assess stability. After 8 days, the $CaCO_3$ particles remained with the initial spherical morphology and size (Figure 6A1),

DOI: 10.1021/am507309t
ACS Appl. Mater. Interfaces 2015, 7, 1735−1745

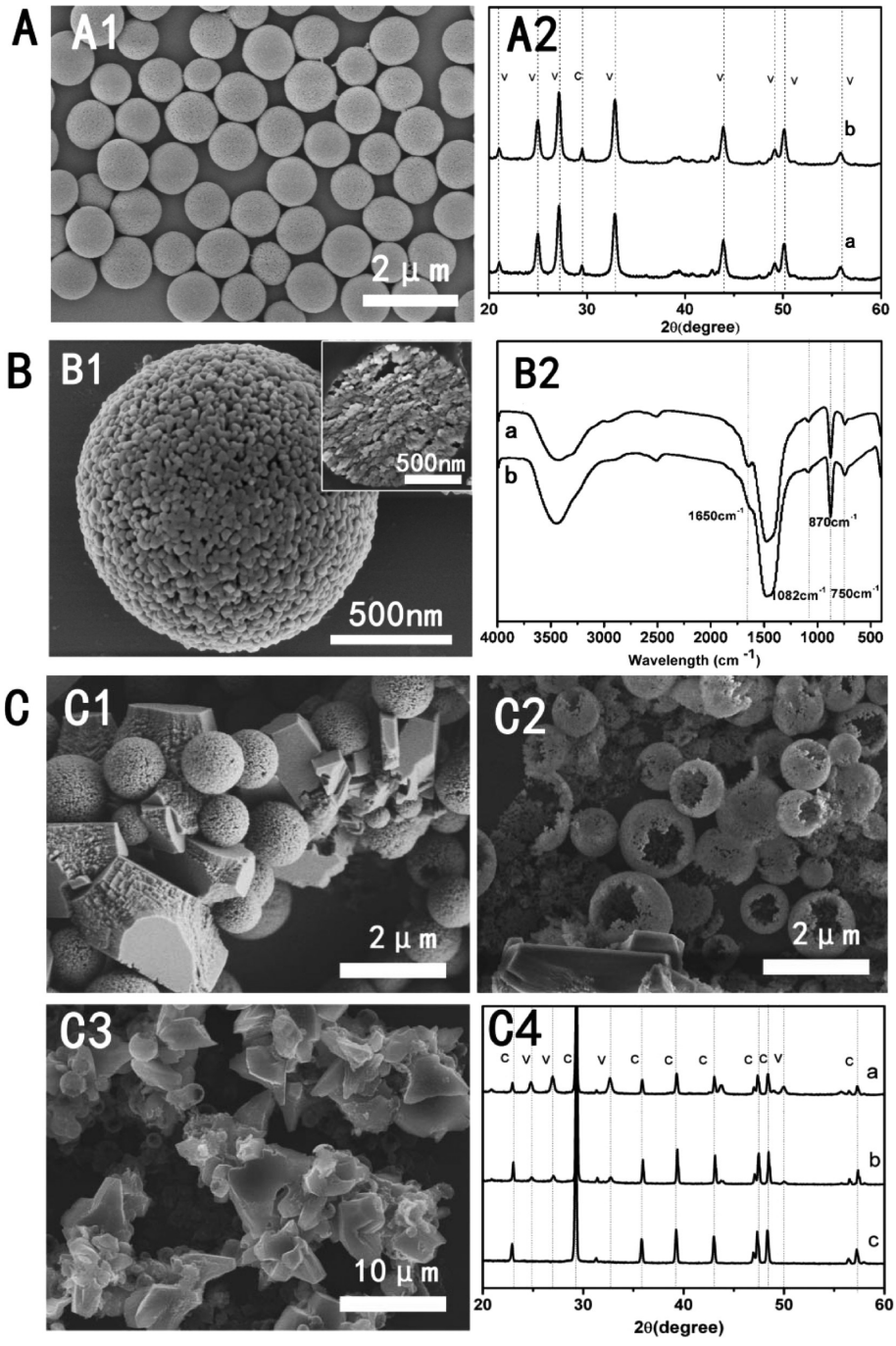

Figure 6. Stability of the vaterite microspheres with and without SF. (A) SEM image of $CaCO_3$ particles containing SF after incubation for 8 days in flowing water solution, and the XRD patterns of the $CaCO_3$ particles before (A2, a) and after (A2, b) incubation. (B) SEM images (B1) and FTIR spectra (B2) of the $CaCO_3$ microsphere after SF removal. (Inset in B1) Cross-section image of the sample while the (B2, a) and (B2, b) of the FTIR curves (B2) indicated the samples before and after SF removal. SF was removed after the treatment at 310 °C for 2 h. (C) SEM images (C1−C3) and XRD patterns (C4) of the $CaCO_3$ particles without SF after incubation for different time in flowing water solution: (C4, a) 2, (C4, b) 4, and (C4, c) 8 days.

suggesting stabilized features. All of the typical vaterite peaks remained, and no calcite peak appeared by XRD after the water flow process (Figure 6A2), confirming the stability of the SF-regulated vaterite microspheres. The electrostatic interaction of the Ca^{2+} and the anionic site of the SF were responsible for the stability of the thermodynamically unfavorable vaterite polymorph.[36] Vaterite microspheres after removal of SF (microspheres were treated at 310 °C for 2 h) were incubated in the same flowing water solution to identify the stabilization effect of SF. After this treatment, a rougher surface and more voids appeared inside the microspheres (Figure 6B1), suggesting the removal of the SF. The disappearance of the peak at 1650 cm^{-1} related to SF further confirmed that most of SF had been eliminated (Figure 6B2). There is no transformation from vaterite to calcite in the process since typical vaterite peaks in FTIR curves remained unchanged after the thermal treatment (Figure 6B2). However, significant transformation from vaterite to calcite occurred after incubation of 2

DOI: 10.1021/am507309t
ACS Appl. Mater. Interfaces 2015, 7, 1735−1745

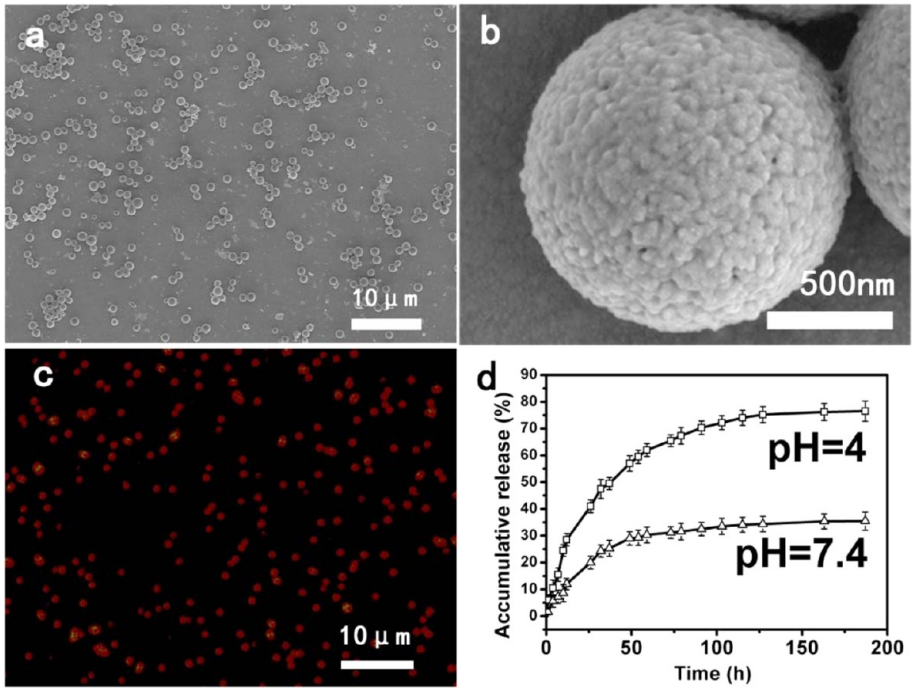

Figure 7. Drug loading and release behavior of the vaterite microspheres. (a) SEM image of the DOX-loaded $CaCO_3$ microspheres. (b) High magnification of the microspheres in a. (c) Fluorescence image of DOX-loaded $CaCO_3$ microspheres. (d) In vitro drug release profiles of DOX-loaded $CaCO_3$ microspheres in different pH medium.

days in the flow of water, and almost all of the vaterite was transformed into calcite after 8 days (Figure 6C), revealing the critical stabilization function of SF.

3.4. Drug Loading and Release From SF-Regulated Vaterite Microspheres. Vaterite is a useful candidate for drug release due to the large surface area, biocompatibility, biodegradability, lower toxicity, low production costs, and pH-dependent dissolution.[50,51] The vaterite particles with smaller and homogeneous sizes are preferred for drug delivery because of their improved efficient and homogeneous distribution of drugs as well as better cell uptake.[52−54] Compared to previous studies, the silk-regulated vaterite microspheres with smaller sizes achieved in our present study, along with the SF-stabilizing features, suggest utility as drug carriers. Nitrogen adsorption results indicated a high surface area of about 54.5 $m^2\ g^{-1}$ and some nanopores (about 5−6 nm) for the vaterite microspheres (Figure S3, Supporting Information). The drug loading and release behavior of the vaterite microspheres were assessed with DOX as a model drug. The strong red fluorescence (Figure 7c) of the DOX-loaded vaterite microspheres indicated the successful and homogeneous loading (Figure 7a and 7b). Absorbance analysis showed that the drug loading content and the entrapment efficiency of DOX was 4.5 ± 0.1% and 93.4 ± 1.7%, respectively, when the ratio of drug and vaterite was 1:20 (w/w), significantly higher than previous results with submicrometer vaterite carriers.[54] Since the submicrometer vaterite carriers have larger specific surface area, the increased drug entrapment efficiency of the microspheres in the present work may be due to the SF embedded in the particles, where the negative charge could form strong electrostatic interaction with DOX.[55−57]

The in vitro release of DOX from the vaterite microspheres at pH 7.4 and 4 is shown in Figure 7d. Due to the stronger interactions of DOX and SF, an initial burst release, as in previous $CaCO_3$-based release systems,[9,52−54,58−62] was significantly reduced, resulting in sustained release for more than 1 week. The DOX release from the microspheres was also strongly pH dependent, higher at pH 4 than at pH 7.4. After 8 days, the amount of DOX released at pH 7.4 was 30% of the total drug load but reached 80% at pH 4. Compared to previous reports,[53] the slower release from the vaterite microspheres suggested stronger interactions between DOX and the microspheres.

4. CONCLUSIONS

Monodisperse vaterite microspheres with smaller sizes can be prepared with SF nanospheres as a modifier. The polymorph and nanostructure of these microspheres were regulated by altering the experimental parameters such as the SF nanostructure and concentration. The vaterite microspheres were stabilized by the SF without transformation into calcite. Higher DOX encapsulation and improved interactions supported sustained drug release and pH-sensitive release behavior, suggesting utility of the vaterite microspheres as drug carriers. The results provide new insight into the relationship between SF and $CaCO_3$ biomineralization as well as a facile, efficient way to rapidly synthesize well-controlled vaterite particles.

■ ASSOCIATED CONTENT

Supporting Information

SEM images of $CaCO_3$ particles obtained in different concentrations of SF at a certain mass ratio ($[Ca^{2+}]$:[SF] = 1:4), EDAX spectrum of the $CaCO_3$ microsphere, nitrogen adsorption/desorption isotherm and pore size distribution for $CaCO_3$ microsphere. This material is available free of charge via the Internet at http://pubs.acs.org.

DOI: 10.1021/am507309t
ACS Appl. Mater. Interfaces 2015, 7, 1735−1745

AUTHOR INFORMATION

Corresponding Authors

*E-mail: dngs008@yahoo.com.cn.
*E-mail: Lvqiang78@suda.edu.cn.

Notes

The authors declare no competing financial interest.

ACKNOWLEDGMENTS

We thank the National Basic Research Program of China (973 Program, 2013CB934400), NSFC (21174097, 81272106, 81271412), and NIH (R01 DE017207). We also thank the Priority Academic Program Development of Jiangsu Higher Education Institutions (PAPD), Excellent Youth Foundation of Jiangsu Province (BK2012009), International S&T Cooperation Project of the Ministry of S&T of China (2010DFR30850), and Key Natural Science Foundation of the Jiangsu Higher Education Institutions of China (11KGA430002) for support of this work.

REFERENCES

(1) Sommerdijk, N. A.; Cusack, M. Biomineralization: Crystals Competing for Space. *Nat. Mater.* **2014**, *13*, 1078−1079.
(2) Chen, C.; Wang, Z.; Saito, M.; Tohei, T.; Takano, Y.; Ikuhara, Y. Fluorine in Shark Teeth: Its Direct Atomic-Resolution Imaging and Strengthening Function. *Angew. Chem., Int. Ed.* **2014**, *53*, 1543−1547.
(3) Addadi, L.; Joester, D.; Nudelman, F.; Weiner, S. Mollusk Shell Formation: A Source of New Concepts for Understanding Biomineralization Processes. *Chem.—Eur. J.* **2006**, *12*, 980−987.
(4) Dorozhkin, S. V. Calcium Orthophosphates in Nature, Biology and Medicine. *Materials* **2009**, *2*, 399−498.
(5) Kabalah-Amitai, L.; Mayzel, B.; Kauffmann, Y.; Fitch, A. N.; Bloch, L.; Gilbert, P. U.; Pokroy, B. Vaterite Crystals Contain Two Interspersed Crystal Structures. *Science* **2013**, *340*, 454−457.
(6) Fratzl, P. Biomimetic Materials Research: What Can We Really Learn from Nature's Structural Materials. *J. R. Soc. Interface* **2007**, *4*, 637−642.
(7) Kim, Y. Y.; Ribeiro, L.; Maillot, F.; Ward, O.; Eichhorn, S. J.; Meldrum, F. C. Bio-Inspired Synthesis and Mechanical Properties of Calcite−Polymer Particle Composites. *Adv. Mater.* **2010**, *22*, 2082−2086.
(8) Guo, H.; Sun, P.; Qin, Z.; Shan, L.; Zhang, G.; Cui, S.; Liang, Y. Sodium Lignosulfonate Induced Vaterite Calcium Carbonate with Multilayered Structure. *Eur. J. Inorg. Chem.* **2014**, 1001−1009.
(9) Yang, Y.-H.; Liu, C.-H.; Liang, Y.-H.; Lin, F.-H.; Wu, K. C.-W. Hollow Mesoporous Hydroxyapatite Nanoparticles (HmHANPs) with Enhanced Drug Loading and PH-Responsive Release Properties for Intracellular Drug Delivery. *J. Mater. Chem. B* **2013**, *1*, 2447−2450.
(10) Schüler, T.; Renkel, J.; Hobe, S.; Susewind, M.; Jacob, D. E.; Panthöfer, M.; Hoffmann-Röder, A.; Paulsen, H.; Tremel, W. Designed Peptides for Biomineral Polymorph Recognition: a Case Study for Calcium Carbonate. *J. Mater. Chem. B* **2014**, *2*, 3511−3518.
(11) Ma, X.; Yuan, S.; Yang, L.; Li, L.; Zhang, X.; Su, C.; Wang, K. Fabrication and Potential Applications of $CaCO_3$−Lentinan Hybrid Materials with Hierarchical Composite Pore Structure Obtained by Self-assembly of Nanoparticles. *CrystEngComm* **2013**, *15*, 8288−8299.
(12) Foran, E.; Weiner, S.; Fine, M. Biogenic Fish-Gut Calcium Carbonate Is a Stable Amorphous Phase in the Gilt-Head Seabream, Sparus Aurata. *Sci. Rep.* **2013**, *3*, 1700−1−1700−5.
(13) Vlieg, E. Complexity from Simplicity. *Science* **2013**, *340*, 822−823.
(14) Choi, C. S.; Kim, Y. W. A Study of the Correlation between Organic Matrices and Nanocomposite Materials in Oyster Shell Formation. *Biomaterials* **2000**, *21*, 213−222.
(15) Liu, Y.; Cui, Y.; Mao, H.; Guo, R. Calcium Carbonate Crystallization in the Presence of Casein. *Cryst. Growth Des.* **2012**, *12*, 4720−4726.
(16) Kim, S.; Park, C. B. Bio-Inspired Synthesis of Minerals for Energy, Environment, and Medicinal Applications. *Adv. Funct. Mater.* **2013**, *23*, 10−25.
(17) Li, X. Q.; Feng, Z.; Xia, Y.; Zeng, H. C. Protein-Assisted Synthesis of Double-Shelled $CaCO_3$ Microcapsules and Their Mineralization with Heavy Metal Ions. *Chem.—Eur. J.* **2012**, *18*, 1945−1952.
(18) Guo, H.; Sun, P.; Qin, Z.; Shan, L.; Zhang, G.; Cui, S.; Liang, Y. Sodium Lignosulfonate Induced Vaterite Calcium Carbonate with Multilayered Structure. *Eur. J. Inorg. Chem.* **2014**, *2014*, 1001−1009.
(19) Tseng, Y. H.; Chevallard, C.; Dauphin, Y.; Guenoun, P. $CaCO_3$ Nanostructured Crystals Induced by Nacreous Organic Extracts. *CrystEngComm* **2014**, *16*, 561−569.
(20) Metzler, R. A.; Evans, J. S.; Killian, C. E.; Zhou, D.; Churchill, T. H.; Appathurai, N. P.; Coppersmith, S. N.; Gilbert, P. Nacre Protein Fragment Templates Lamellar Aragonite Growth. *J. Am. Chem. Soc.* **2010**, *132*, 6329−6334.
(21) Wang, S. S.; Xu, A. W. Amorphous Calcium Carbonate Stabilized by a Flexible Biomimetic Polymer Inspired by Marine Mussels. *Cryst. Growth Des.* **2013**, *13*, 1937−1942.
(22) Li, H.; Xin, H. L.; Muller, D. A.; Estroff, L. A. Visualizing the 3D Internal Structure of Calcite Single Crystals Grown in Agarose Hydrogels. *Science* **2009**, *326*, 1244−1247.
(23) Mann, S.; Ozin, G. A. Synthesis of Inorganic Materials with Complex Form. *Nature* **1996**, *382*, 313−318.
(24) Raiteri, P.; Gale, J. D. Water Is the Key to Nonclassical Nucleation of Amorphous Calcium Carbonate. *J. Am. Chem. Soc.* **2010**, *132*, 17623−17634.
(25) Kim, Y. Y.; Ganesan, K.; Yang, P.; Kulak, A. N.; Borukhin, S.; Pechook, S.; Ribeiro, L.; Kröger, R.; Eichhorn, S. J.; Armes, S. P. An Artificial Biomineral Formed by Incorporation of Copolymer Micelles in Calcite Crystals. *Nat. Mater.* **2011**, *10*, 890−896.
(26) Wang, S. S.; Picker, A.; Cölfen, H.; Xu, A. W. Heterostructured Calcium Carbonate Microspheres with Calcite Equatorial Loops and Vaterite Spherical Cores. *Angew. Chem., Int. Ed.* **2013**, *52*, 6317−6321.
(27) Naka, K.; Huang, S. C.; Chujo, Y. Formation of Stable Vaterite with Poly (Acrylic Acid) by the Delayed Addition Method. *Langmuir* **2006**, *22*, 7760−7767.
(28) Chen, S. F.; Yu, S. H.; Wang, T. X.; Jiang, J.; Cölfen, H.; Hu, B.; Yu, B. Polymer-Directed Formation of Unusual $CaCO_3$ Pancakes with Controlled Surface Structures. *Adv. Mater.* **2005**, *17*, 1461−1465.
(29) Hao, W.; Porter, D.; Wang, X.; Shao, Z. Silk Fibroin-Mediated Biomineralization of Calcium Carbonate at the Air/Water Interface. *CrystEngComm* **2014**, *16*, 9176−9184.
(30) Zhao, R. B.; Han, H. F.; Ding, S.; Li, Z. H.; Kong, X. D. Effect of Silk Sericin on Morphology and Structure of Calcium Carbonate Crystal. *Front. Mater. Sci.* **2013**, *7*, 177−183.
(31) Ming, J.; Zuo, B. Crystal Growth of Calcium Carbonate in Silk Fibroin/Sodium Alginate Hydrogel. *J. Cryst. Growth* **2014**, *386*, 154−161.
(32) Wu, Y.; Cheng, C.; Yao, J.; Chen, X.; Shao, Z. Crystallization of Calcium Carbonate on Chitosan Substrates in the Presence of Regenerated Silk Fibroin. *Langmuir* **2011**, *27*, 2804−2810.
(33) Wang, T.; Che, R.; Li, W.; Mi, R.; Shao, Z. Control over Different Crystallization Stages of $CaCO_3$-Mediated by Silk Fibroin. *Cryst. Growth Des.* **2011**, *11*, 2164−2171.
(34) Wang, T.; Porter, D.; Shao, Z. The Intrinsic Ability of Silk Fibroin to Direct the Formation of Diverse Aragonite Aggregates. *Adv. Funct. Mater.* **2012**, *22*, 435−441.
(35) Keene, E. C.; Evans, J. S.; Estroff, L. A. Silk Fibroin Hydrogels Coupled with the N16N-β-Chitin Complex: An in Vitro Organic Matrix for Controlling Calcium Carbonate Mineralization. *Cryst. Growth Des.* **2010**, *10*, 5169−5175.
(36) Cheng, C.; Shao, Z.; Vollrath, F. Silk Fibroin-Regulated Crystallization of Calcium Carbonate. *Adv. Funct. Mater.* **2008**, *18*, 2172−2179.
(37) Zhang, X.; Fan, Z.; Lu, Q.; Huang, Y.; Kaplan, D. L.; Zhu, H. Hierarchical Biomineralization of Calcium Carbonate Regulated by Silk Microspheres. *Acta Biomater.* **2013**, *9*, 6974−6980.

DOI: 10.1021/am507309t
ACS Appl. Mater. Interfaces 2015, 7, 1735−1745

(38) Xu, S.; Wu, P. Monodisperse Spherical $CaCO_3$ Superstructure Self-assembled by Vaterite Lamella under Control of Regenerated Silk Fibroin *via* Compressed CO_2. *CrystEngComm* **2013**, *15*, 5179−5188.
(39) Xu, S.; Wu, P. A Aapid, Green and Versatile Route to Synthesize Metal Carbonate Superstructures *via* the Combination of Regenerated Silk Fibroin and Compressed CO_2. *CrystEngComm* **2014**, *16*, 1311−1321.
(40) Lu, Q.; Zhu, H.; Zhang, C.; Zhang, F.; Zhang, B.; Kaplan, D. L. Silk Self-Assembly Mechanisms and Control from Thermodynamics to Kinetics. *Biomacromolecules* **2012**, *13*, 826−832.
(41) Xu, A. W.; Antonietti, M.; Cölfen, H.; Fang, Y. P. Uniform Hexagonal Plates of Vaterite $CaCO_3$ Mesocrystals Formed by Biomimetic Mineralization. *Adv. Funct. Mater.* **2006**, *16*, 903−908.
(42) Dong, W.; Tu, C.; Tao, W.; Zhou, Y.; Tong, G.; Zheng, Y.; Li, Y.; Yan, D. Influence of the Mole Ratio of the Interacting to the Stabilizing Portion ($R_{I/S}$) in Hyperbranched Polymers on $CaCO_3$ Crystallization: Synthesis of Highly Monodisperse Microspheres. *Cryst. Growth Des.* **2012**, *12*, 4053−4059.
(43) Wang, Y.; Moo, Y. X.; Chen, C.; Gunawan, P.; Xu, R. Fast Precipitation of Uniform $CaCO_3$ Nanospheres and Their Transformation to Hollow Hydroxyapatite Nanospheres. *J. Colloid Interface Sci.* **2010**, *352*, 393−400.
(44) Rockwood, D. N.; Preda, R. C.; Yücel, T.; Wang, X.; Lovett, M. L.; Kaplan, D. L. Materials Fabrication from *Bombyx Mori* Silk Fibroin. *Nat. Protoc.* **2011**, *6*, 1612−1631.
(45) Lu, Q.; Huang, Y.; Li, M.; Zuo, B.; Lu, S.; Wang, J.; Zhu, H.; Kaplan, D. L. Silk Fibroin Electrogelation Mechanisms. *Acta Biomater.* **2011**, *7*, 2394−2400.
(46) Cölfen, H.; Antonietti, M. Crystal Design of Calcium Carbonate Microparticles Using Double-Hydrophilic Block Copolymers. *Langmuir* **1998**, *14*, 582−589.
(47) Wang, T.; Cölfen, H.; Antonietti, M. Nonclassical Crystallization: Mesocrystals and Morphology Change of $CaCO_3$ Crystals in the Presence of a Polyelectrolyte Additive. *J. Am. Chem. Soc.* **2005**, *127*, 3246−3247.
(48) López-Macipe, A.; Gómez-Morales, J.; Rodríguez-Clemente, R. Calcium Carbonate Precipitation from Aqueous Solutions Containing Aerosol OT. *J. Cryst. Growth* **1996**, *166*, 1015−1019.
(49) Naka, K.; Tanaka, Y.; Chujo, Y. Effect of Anionic Starburst Dendrimers on the Crystallization of $CaCO_3$ in Aqueous Solution: Size Control of Spherical Vaterite Particles. *Langmuir* **2002**, *18*, 3655−3658.
(50) Parakhonskiy, B. V.; Haase, A.; Antolini, R. Sub-Micrometer Vaterite Containers: Synthesis, Substance Loading, and Release. *Angew. Chem., Int. Ed.* **2012**, *51*, 1195−1197.
(51) Schmidt, S.; Volodkin, D. Microparticulate Biomolecules by Mild $CaCO_3$ Templating. *J. Mater. Chem. B* **2013**, *1*, 1210−1218.
(52) Qi, C.; Zhu, Y. J.; Chen, F. Microwave Hydrothermal Transformation of Amorphous Calcium Carbonate Nanospheres and Application in Protein Adsorption. *ACS Appl. Mater. Interfaces* **2014**, *6*, 4310−4320.
(53) Wang, J.; Chen, J.-S.; Zong, J.-Y.; Zhao, D.; Li, F.; Zhuo, R.-X.; Cheng, S.-X. Calcium Carbonate/Carboxymethyl Chitosan Hybrid Microspheres and Nnanospheres for Drug Delivery. *J. Phys. Chem. C* **2010**, *114*, 18940−18945.
(54) Wei, W.; Ma, G. H.; Hu, G.; Yu, D.; McLeish, T.; Su, Z. G.; Shen, Z. Y. Preparation of Hierarchical Hollow $CaCO_3$ Particles and the Application as Anticancer Drug Carrier. *J. Am. Chem. Soc.* **2008**, *130*, 15808−15810.
(55) Seib, F. P.; Jones, G. T.; Rnjak-Kovacina, J.; Lin, Y.; Kaplan, D. L. pH-Dependent Anticancer Drug Release from Silk Nanoparticles. *Adv. Healthcare Mater.* **2013**, *2*, 1606−1611.
(56) Seib, F. P.; Pritchard, E. M.; Kaplan, D. L. Self-Assembling Doxorubicin Silk Hydrogels for the Focal Treatment of Primary Breast Cancer. *Adv. Funct. Mater.* **2013**, *23*, 58−65.
(57) Subia, B.; Chandra, S.; Talukdar, S.; Kundu, S. C. Folate Conjugated Silk Fibroin Nanocarriers for Targeted Drug Delivery. *Integr. Biol.* **2014**, *6*, 203−214.
(58) Ying, X.; Shan, C.; Jiang, K.; Chen, Z.; Du, Y. Intracellular pH-Sensitive Delivery $CaCO_3$ Nanoparticles Templated by Hydrophobic Modified Starch Micelles. *RSC Adv.* **2014**, *4*, 10841−10844.
(59) Kurapati, R.; Raichur, A. M. Composite Cyclodextrin−Calcium Carbonate Porous Microparticles and Modified Multilayer Capsules: Novel Carriers for Encapsulation of Hydrophobic Drugs. *J. Mater. Chem. B* **2013**, *1*, 3175−3184.
(60) Peng, C.; Zhao, Q.; Gao, C. Sustained Delivery of Doxorubicin by Porous $CaCO_3$ and Chitosan/Alginate Multilayers-Coated $CaCO_3$ Microparticles. *Colloids Surf., A* **2010**, *353*, 132−139.
(61) Parakhonskiy, B. V.; Foss, C.; Carletti, E.; Fedel, M.; Haase, A.; Motta, A.; Migliaresi, C.; Antolini, R. Tailored Intracellular Delivery *via* a Crystal Phase Transition in 400 nm Vaterite Particles. *Biomater. Sci.* **2013**, *1*, 1273−1281.
(62) Svenskaya, Y.; Parakhonskiy, B.; Haase, A.; Atkin, V.; Lukyanets, E.; Gorin, D.; Antolini, R. Anticancer Drug Delivery System Based on Calcium Carbonate Particles Loaded with a Photosensitizer. *Biophys. Chem.* **2013**, *182*, 11−15.

DOI: 10.1021/am507309t
ACS Appl. Mater. Interfaces 2015, 7, 1735−1745